Biomech Model Mechanobiol
DOI 10.1007/s10237-017-0981-8

ORIGINAL PAPER

Incorporating tissue anisotropy and heterogeneity in finite element models of trabecular bone altered predicted local stress distributions

Max A. Hammond[1] · **Joseph M. Wallace**[2] · **Matthew R. Allen**[3] · **Thomas Siegmund**[1]

Received: 25 July 2017 / Accepted: 1 November 2017

Abstract Trabecular bone is composed of organized mineralized collagen fibrils, which results in heterogeneous and anisotropic mechanical properties at the tissue level. Recently, biomechanical models computing stresses and strains in trabecular bone have indicated a significant effect of tissue heterogeneity on predicted stresses and strains. However, the effect of the tissue-level mechanical anisotropy on the trabecular bone biomechanical response is unknown. Here, a computational method was established to automatically impose physiologically relevant orientation inherent in trabecular bone tissue on a trabecular bone microscale finite element model. Spatially varying tissue-level anisotropic elastic properties were then applied according to the bone mineral density and the local tissue orientation. The model was used to test the hypothesis that anisotropy in both homogeneous and heterogeneous models alters the predicted distribution of stress invariants. Linear elastic finite element computations were performed on a 3 mm cube model isolated from a microcomputed tomography scan of human trabecular bone from the distal femur. Hydrostatic stress and von Mises equivalent stress were recorded at every element, and the distributions of these values were analyzed. Anisotropy reduced the range of hydrostatic stress in both tension and compression more strongly than the associated increase in von Mises equivalent stress. The effect of anisotropy was independent of the spatial redistribution high compressive stresses due to tissue elastic heterogeneity. Tissue anisotropy and heterogeneity are likely important mechanisms to protect bone from failure and should be included for stress analyses in trabecular bone.

Keywords Microcomputed tomography · Collagen fiber orientation · Anisotropy · Stress analysis

1 Introduction

Human trabecular bone has a complex 3D microstructure that results in anisotropy on a microstructural level as trabeculae mainly align with the principal loading direction. In addition, the nanostructure of trabecular tissue also gives rise to anisotropy on the tissue level. Trabecular tissue is composed of mineralized collagen fibrils organized into lamellar trabecular packets. Trabecular packets are formed during bone turnover by osteoblasts depositing collagen along the surface of hemispherical resorption cavities. This leads to a collagen structure largely aligned along the long axis of the trabeculae approximately in-plane with its surface (Reznikov et al. 2015; Georgiadis et al. 2016). Due to this alignment of collagen fibrils, bone is a highly anisotropic material at the tissue level. Because remodeling acts on the surface of the trabeculae and the mean thickness of trabecular packets is less than the trabecular thickness, older tissue is preferentially preserved in the interior of the trabeculae (Lips et al. 1978; Torres et al.

This material was based upon work supported by the National Science Foundation under Grant No. 1643164.

Electronic supplementary material The online version of this article (https://doi.org/10.1007/s10237-017-0981-8) contains supplementary material, which is available to authorized users.

✉ Thomas Siegmund
siegmund@purdue.edu

[1] School of Mechanical Engineering, Purdue University, 585 Purdue Mall, West Lafayette, IN 47907, USA

[2] Department of Biomedical Engineering, Indiana University-Purdue Universitry Indianapolis, Indianapolis, IN 46202, USA

[3] Department of Anatomy and Cell Biology, Indiana University School of Medicine, Indianapolis, IN 46202, USA

Published online: 14 November 2017

2016), and due to the continuing effects of secondary mineralization, this older tissue has higher mineral content than newly formed tissue on the surface of the bone (Liu et al. 2012). This effect of varying mineralization between trabecular packets and variations in mineralization within trabecular packets creates a highly heterogeneous material.

Despite trabecular tissue being highly anisotropic and heterogeneous, finite element (FE) models of trabecular bone commonly assume an isotropic homogeneous tissue (Burr 2016; Engelke et al. 2016). Recent studies have highlighted the shortcomings of such an assumption and have demonstrated the importance of heterogeneity in the elastic modulus of trabecular bone tissue on the predictions of stress and strain obtained in such biomechanical models (Van der Linden et al. 2001; Jaasma et al. 2002; Kaynia et al. 2015; Renders et al. 2008). However, it is unknown how anisotropy in the elastic behavior of the bone tissue affects the stress state in trabecular bone.

The lack of studies that account for anisotropy in trabecular bone tissue can be attributed to the complex structure of trabecular bone and to the number of trabeculae in a typical sample, which makes orientation assignment difficult and manual assignment prohibitive practically. Here, the orientation assignment in trabecular bone tissue was automated by custom software code in MATLAB. This approach has the potential to open the field of trabecular bone FE modeling to the study of sample specific anisotropic tissue-level properties.

Given that anisotropy plays an important role in the stress distribution and the function of other collagen-based or mineralized tissues (Kelleher et al. 2013; Spears et al. 1993; Vande Geest et al. 2008), the collagen fibril alignment and the resulting anisotropy likely play a substantial role in the stress distribution and biomechanical function of trabecular bone tissue as well. Therefore, it was hypothesized that including tissue anisotropy and heterogeneity in a continuum model of the stress–strain response of human trabecular bone would alter the predicted distribution of both the von Mises equivalent stress and the hydrostatic stress along with the associated stress triaxiality to protect the specimen from failure.

2 Materials and methods

2.1 Sample specimen and preparation

The tissue specimen was obtained through the Indiana University School of Medicine Anatomical Education Donor Program. A trabecular core from the distal femur of a human cadaver was imaged with a Skyscan 1172 μCT system (Bruker μCT, Kontich, Belgium) with an isotropic voxel size of 5.88 μm. NRecon (Bruker μCT) was used to reconstruct voxels in the 0–0.11 mm^{-1} range, and Dataviewer (Bruker μCT) was used to vertically align the images. Manufacturer-supplied hydroxyapatite phantoms of 250 and 750 kg/m^3 were used to calculate the mineral density (ρ) of each gray scale (GS) using the linear relationship $\rho_{GS} = 11.1\,kg/m^3 \times GS - 255\,kg/m^3$ derived from a linear fit of the gray scales of the phantoms. Using CTAn (Bruker μCT), a 3.00 mm cube region of interest was selected from the interior of the scan to which Gaussian smoothing was applied. The Otsu method was used to determine the threshold to separate bone from marrow. The average gray scale within the bone volume, bone volume fraction, trabecular thickness, trabecular separation, degree of anisotropy (i.e., the alignment of trabeculae at the microstructural level), and connectivity density was calculated using CTAn. The sample had a trabecular microarchitecture that was typical of the distal femur (Table 1) (Patel et al. 2003). ScanIP (Simpleware, Exeter, UK) was used to generate a free continuum mesh of the trabecular bone volume, and the average gray scale of the voxels contained in each element was recorded.

Table 1 Trabecular microarchitecture and density of the sample

	Mean
Bone volume fraction	18.2%
Trabecular thickness	68.3 μm
Trabecular separation	597 μm
Trabecular number	2.66 m^{-1}
Connectivity density	55.8 m^{-3}
Degree of anisotropy	0.627
Average density of hydroxyapatite	964 kg/m^{-3}

2.2 Applying tissue properties

For the isotropic models considered, the elastic modulus (E) was 5 GPa and the Poisson's ratio (ν) was 0.37, which were within the expected range for hydrated trabecular bone (Rho et al. 1998; Ashman et al. 1984). Shear modulus (G) was defined as $G = E/(2 + 2\nu)$. For the anisotropic models, directionality was introduced by calculating a local ijk-coordinate system for every element (Fig. 1). In order to calculate the local coordinate system, the mesh generated in ScanIP was imported into MATLAB (MathWorks, Natick, MA). A custom-written MATLAB code was then used to assign tissue anisotropy and heterogeneity. The normal to each triangular surface face on the exterior of the trabeculae was calculated using the cross product of two sides of the triangular surface. Surface faces along the sides of the cube were not treated as part of the exterior trabecular surface because this surface was produced artificially and was not part of the native trabecular surface. A local coordinate system was then defined with the surface normal as the local i-axis so that the surface face would be in the jk-

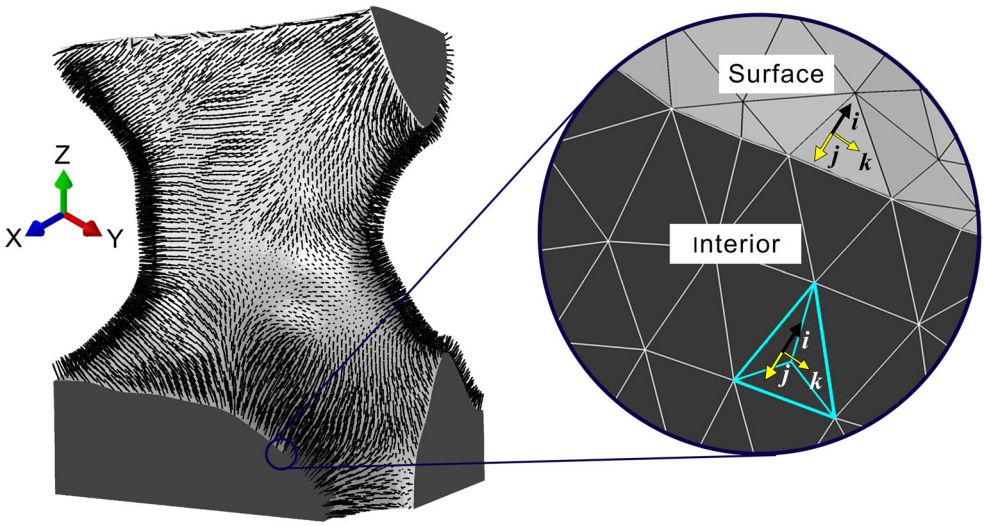

Fig. 1 Anisotropy was defined using a local coordinate for each element calculated independently of the global XYZ-coordinate system. The normal (black arrows) of each surface element was calculated with the cube boundaries at the XYZ limits treated as the interior as shown in the trabecula on the left. A local ijk-coordinate system was assigned with the surface normal along the local i-axis and the local j- and k-axes (yellow arrows) defined the assumed collagen fibril plane. As shown in the inset, the highlighted interior element is assigned the closest surface coordinate system calculated from the centroid of the element to the centroid of the surface face

plane. The distance between the element centroid and the centroid of all the triangular surface faces was calculated for every element without a face on the trabecular surface. The local coordinate system of the nearest surface was then applied to each element not on the surface and the distance between the element and surface centroid was recorded as the trabecular depth. Following the definition of a local coordinate system for each element, transversely isotropic tissue properties were assigned with symmetry in the local jk-plane. Computations were considered with $2E_i = E_j = E_k$, $\nu_{jk} = 1.25\nu_{ji} = 0.37$, and $G_{jk} = 1.5G_{ji}$ as well as $3E_i = E_j = E_k$, $\nu_{jk} = 1.25\nu_{ji} = 0.37$, and $G_{jk} = 1.75G_{ji}$. The ratios selected for E, ν, and G between the i- and jk-directions were physiologically relevant as similar values in the i-direction and the average of the jk-directions were observed experimentally (Reisinger et al. 2011).

For the homogeneous models, tissue properties depended solely on the isotropic and anisotropic definitions. For the heterogeneous isotropic and anisotropic models, E and E_i, respectively, were adjusted relative to the grayscale information from the μCT scan. The average density of the region of interest (ρ_{Avg}) was calculated using the average gray scale in the bone volume and the previously defined relationship between gray scale and density derived from the hydroxyapatite phantoms ($\rho_{\mathrm{GS}} = 11.1\ \mathrm{kg/m^3} \times \mathrm{GS} - 255\ \mathrm{kg/m^3}$). In addition, the average gray scale of the voxels contained in each element was recorded. Modulus was calculated for each spatially varying ρ_{GS} and the overall ρ_{Avg} (both with units of $\mathrm{kg/m^3}$) using $E = 4.56\mathrm{m^2/s^2} \times \rho - 331\mathrm{MPa}$ from Rho et al (Rho et al. 1995) in order to compute scaling factor α, where $\alpha = E(\rho_{\mathrm{GS}})/E(\rho_{\mathrm{Avg}})$. In every element of the isotropic heterogeneous model, the modulus of the isotropic homogeneous model (5 GPa) was adjusted by the ratio α. In every element of the anisotropic heterogeneous model, the E_i from the anisotropic homogeneous model was adjusted by the same ratio α. Poisson's ratio was not altered by heterogeneity in either the isotropic or anisotropic case. As shear modulus is defined by E and ν, varying E or E_i dictated the effect of heterogeneity on G or G_{jk}, respectively. The distri-

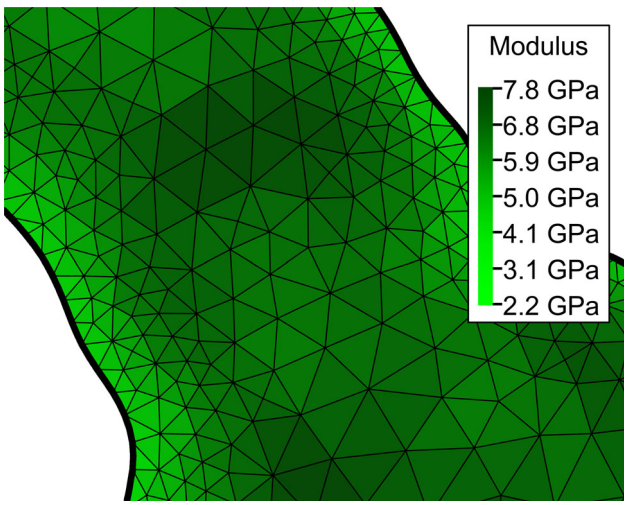

Fig. 2 Distribution of modulus (either isotropic or in the jk-plane) across a representative heterogeneous trabecula. The thick black line is the boundary of the trabecular surface, and the small black lines represent the finite element mesh. Elements near the trabecular surface were less stiff compared to elements further into the interior of the trabeculae. Isolated regions within the interior were stiffer than the surrounding bone, and these regions were primarily deep within the trabeculae

bution of modulus across the span of a trabecula indicated a stiffer region in the trabecular interior (Fig. 2).

2.3 Simulation and analysis

The finite element mesh consisted of 2,544,945 fully integrated 10 node tetrahedral elements of with minimum edge length of 13.2 μm and a maximum edge length of 32.3 μm. As shown in Fig. 2, 15–20 elements span each trabecula and this is sufficient to ensure convergence in an elastic stress analysis (Benzley et al. 1995). Elements were placed into four groups based on their trabecular depth. Surface-near elements were defined as elements with an exposed surface face or ones with a centroid within one voxel (5.88 μm) from the surface. The remaining elements were split evenly into near superficial, interior, and deep groups based on the quantiles of the distribution of trabecular depth. Approximately 30% of all elements were located on or within one voxel (5.88 μm) of the surface and were included in the surface-near group, whereas all other groups contained 23% of the elements. The superficial elements were defined as elements between 5.88 and 15.13 μm, which from the distribution of trabecular thickness (Fig. 3), very few were located at the center of thin trabeculae. The interior elements were defined as between 15.13 and 31.91 μm to include elements in the center of less than average thickness trabeculae. Deep elements were defined as greater than 31.91 μm from the trabecular surface, which encompassed elements within the center of the 68.3 μm average trabecular thickness. The percentage of bone volume contained in the surface-near, superficial, interior, and deep element groups was 10.6, 13.1, 25.6, and 50.6%, respectively. Four combinations of anisotropy ($2E_i = E_j = E_k$) and heterogeneity were considered: isotropic and homogeneous (*IsoHmg*), isotropic and heterogeneous (*IsoHtg*), anisotropic and homogeneous (*AnisoHmg*), and anisotropic and heterogeneous (*AnisoHtg*). In addition, the anisotropy ratio was varied for the heterogeneous case which considered $3E_i = E_j = E_k$. The simulations consider a linear, small deformation analysis that simulated compression along the vertical axis of the specimen. A pressure ($t_0 = 5$MPa) was applied to the upper transaxial surface of the analysis domain and displacements in all directions except the axial direction were constrained. The upper transaxial surface was also constrained to remain parallel to its initial position. All nodes on the opposite surface of the analysis domain were fully constrained, while all other external surfaces of the analysis domain remained free. The von Mises equivalent stress (σ_{Eq}) and hydrostatic stress (σ_{Hyd}) were recorded at the centroid of every element. The values and spatial distribution of the stress invariants were compared between the combinations. The maximum and minimum hydrostatic stress, maximum von Mises equivalent stress, bone volume experiencing either pure tension or compression, and apparent modulus were calculated for each model. The commercial FE code ABAQUS/Standard v2017 (Dassault Systèmes SIMULIA, Johnston, RI) was employed for the simulation.

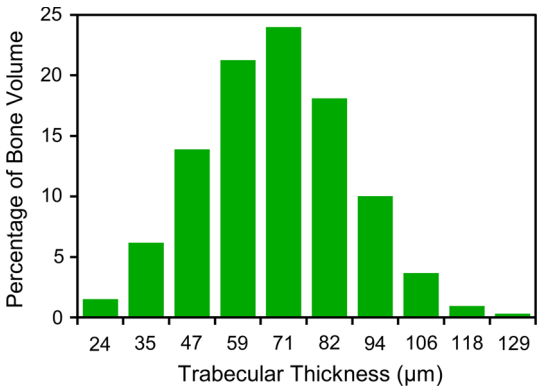

Fig. 3 Distribution of bone volume with respect to trabecular thickness

3 Results

3.1 Heterogeneity shifts high stresses to interior

Contour plots of σ_{Eq} and σ_{Hyd} were used to visualize data in distribution center (Figs. 4 and 5). Scatter plots of σ_{Eq} vs σ_{Hyd} were generated for each respective model/depth group to visualize the values and spatial distribution of von Mises equivalent stress and hydrostatic stress (Figs. 6, 7, 8, and Online Resource Supplemental Fig 1). Lines of constant stress triaxiality (defined as $T = \sigma_{\mathrm{Hyd}}/\sigma_{\mathrm{Eq}}$) at $T = +1/3$ and $T = -1/3$ were included as a visual guide to allow an assessment of the deviation from the uniaxial stress states of tension and compression, respectively. In the isotropic case with homogeneous tissue properties, most elements were contained in a point cloud bound by $\sigma_{\mathrm{Hyd}} = [-2.0, 3.0]$ MPa and $\sigma_{\mathrm{Eq}} = [0.0, 2.5]$ MPa (*IsoHmg*, Fig. 6). The overall mode of deformation was compressive as most recorded stress states are in a negative hydrostatic stress domain, but there are also a significant number of elements experiencing positive hydrostatic pressure (Fig. 5). This finding is the result of an overall compressive stress state in trabeculae aligned with the load axis and the combination of the tension/compression/shear stresses induced by bending of non-aligned trabeculae. For the two domains closest to the surface, there is a set of elements possessing high von Mises equivalent stress (up to 5.0 MPa) at a negative hydrostatic stress value. These stress states follow the uniaxial compression line of $T = -1/3$ and represent 0.126 mm^3 of bone volume. Adding heterogeneity to the isotropic model removed the high uniaxial stress states from the surface-near and superficial elements and reduced the bone volume

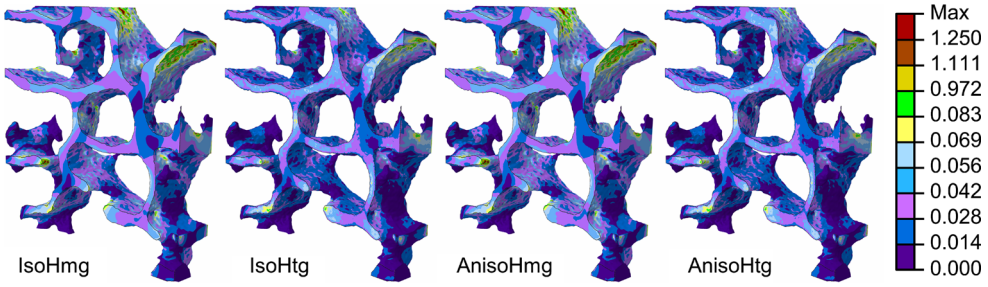

Fig. 4 Contour plots of von Mises equivalent stress highlight the removal of the moderate stress regions at the surface in the heterogeneous models and the minimal effects of anisotropy for the center of the stress distribution

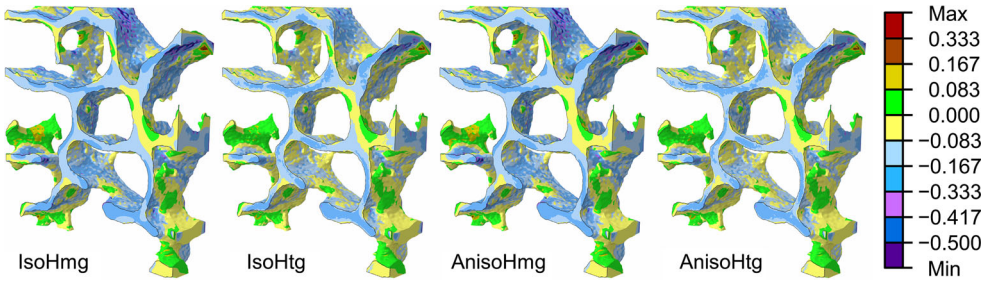

Fig. 5 Contour plots of hydrostatic stress highlight the removal of the high tensile regions at the surface in the heterogeneous models and the minimal effects of anisotropy for values in the center of the hydrostatic stress

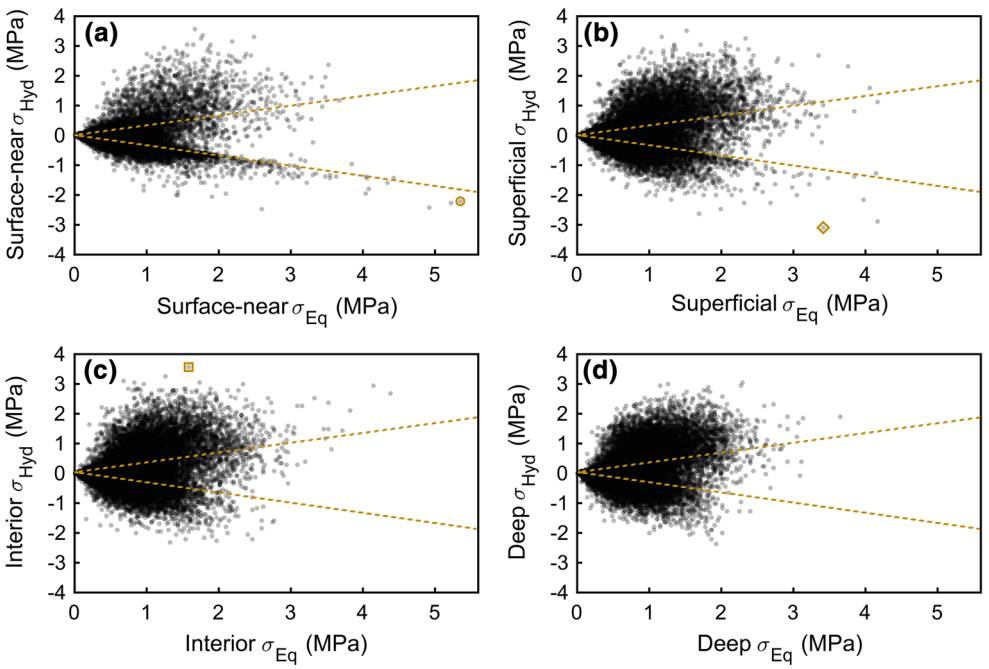

Fig. 6 Isotropic homogeneous model: hydrostatic stress vs von Mises equivalent stress for elements in the **a** surface-near, **b** superficial, **c** interior, and **d** deep elements with maximum von Mises equivalent stress (circle), maximum hydrostatic stress (square), and the minimum hydrostatic stress (diamond) in the model labeled

experiencing pure tension or compression by 2% as well. Adding heterogeneity also shifted the extreme values of σ_{Eq} deeper into the trabeculae while preserving the overall shape of the stress data cloud at lower σ_{Hyd} and σ_{Eq} values (*IsoHtg*, Fig. 7). However, as shown in Figs. 4 and 5, heterogeneity affected this region as well causing the shift of the local moderately extreme regions of σ_{Hyd} and σ_{Eq} away from the trabecular surface. In the anisotropic case, a similar

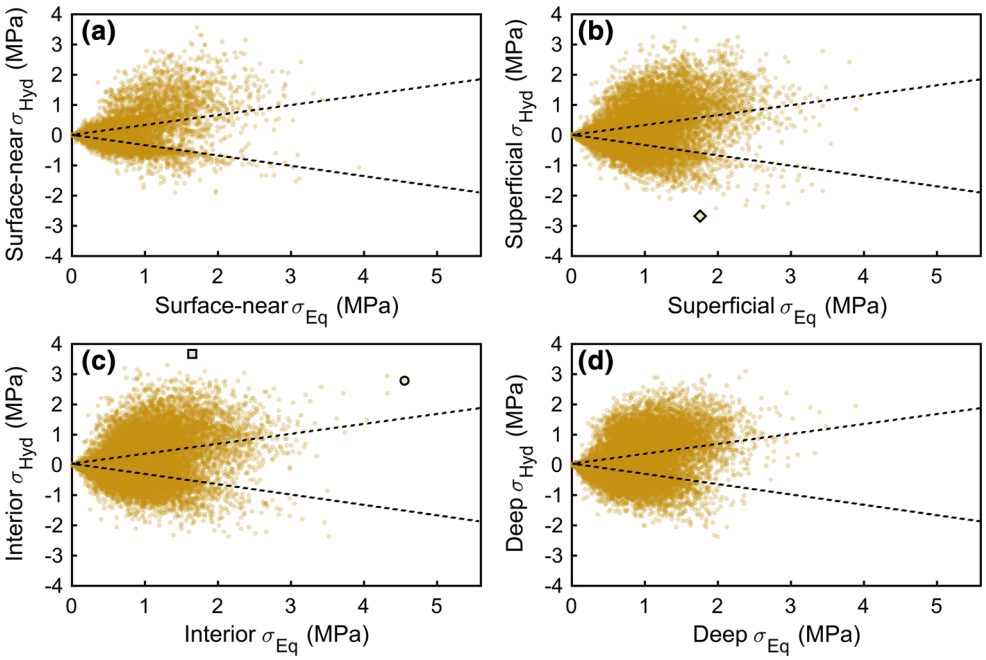

Fig. 7 Isotropic heterogeneous model: hydrostatic stress vs von Mises equivalent stress for elements in the **a** surface-near, **b** superficial, **c** interior, and **d** deep elements with maximum von Mises equivalent stress (circle), maximum hydrostatic stress (square), and the minimum hydrostatic stress (diamond) in the model labeled

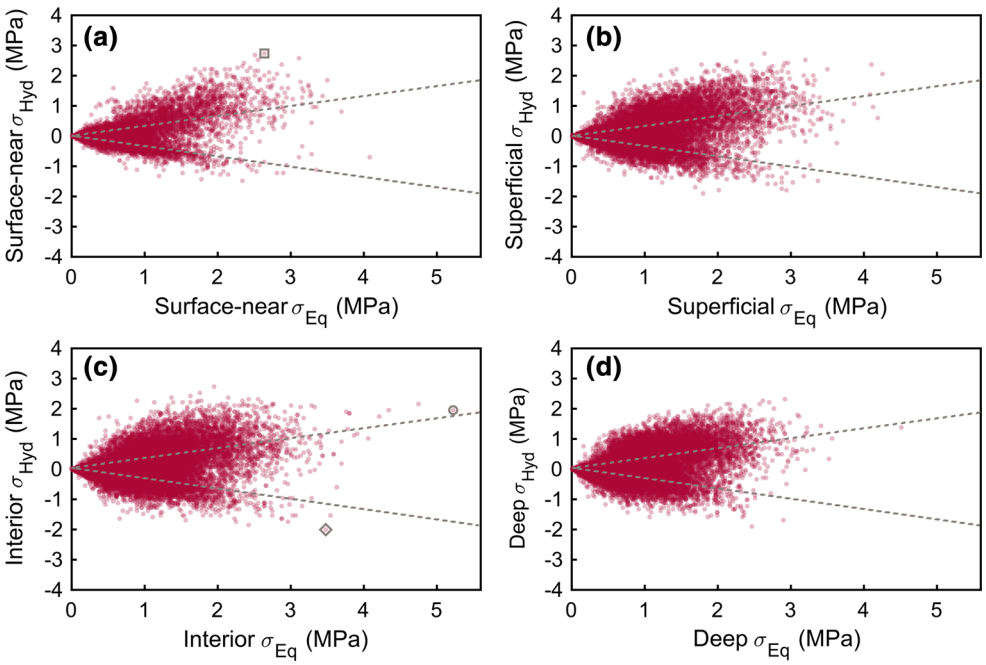

Fig. 8 Anisotropic heterogeneous model: hydrostatic stress vs von Mises equivalent stress for elements in the **a** surface-near, **b** superficial, **c** interior, and **d** deep elements with maximum von Mises equivalent stress (circle), maximum hydrostatic stress (square), and the minimum hydrostatic stress (diamond) in the model labeled

redistribution was observed when comparing the homogeneous and heterogeneous models (*AnisoHmg* vs *AnisoHtg*). Surface-near and superficial elements with high stresses in the uniaxial compression configuration are present in the homogeneous case (Online Resource Supplemental Fig 1), but are removed when heterogeneity was added (Fig. 8) with

the associated 2% decrease in bone volume under uniaxial tension or compression. The apparent modulus was reduced in both isotropic (*IsoHtg*: 50.5 MPa, *IsoHmg*: 53.6 MPa) and anisotropic models (*AnisoHtg*: 48.4 MPa, *AnisoHmg*: 51.3 MPa) when heterogeneity was added by 6%.

3.2 Anisotropy reduces hydrostatic stress and increases von Mises equivalent stress

While depth dependence of the σ_{Hyd}–σ_{Eq} distribution was similar between the isotropic and anisotropic models, adding anisotropy to the models resulted in other substantial differences between the isotropic and anisotropic models. The key differences in the σ_{Hyd}–σ_{Eq} distributions were the reduced the range of hydrostatic stress present in the anisotropic models and the approximately 2.5% average increase in bone volume experiencing uniaxial tension or compression (*AnisoHmg* and *AnisoHtg*). For these models, the stress data cloud was bound by $\sigma_{\mathrm{Hyd}} = [-1.5, 2.0]$ MPa and $\sigma_{\mathrm{Eq}} = [0.0, 2.5]$ MPa, while in the homogeneous cases the data cloud was bound by $\sigma_{\mathrm{Hyd}} = [-2.0, 3.0]$ MPa and $\sigma_{\mathrm{Eq}} = [0.0, 2.5]$ MPa (Online Resource Supplemental Fig 1 and Fig. 8). The extreme values of the anisotropic models experienced a similar shift as the maximum σ_{Hyd} decreased by about 24% (*IsoHmg*: 3.56 MPa, *IsoHtg*: 3.65 MPa, *AnisoHmg*: 2.72 MPa, *AnisoHtg*: 2.74 MPa) and the minimum σ_{Eq} increased by about 25% (*IsoHmg*: − 3.08 MPa, *IsoHtg*: − 2.70 MPa, *AnisoHmg*: − 2.29 MPa, *AnisoHtg*: − 2.02 MPa). The location of the maximum and minimum values of σ_{Hyd} also changed when anisotropy was added and was shifted to a different trabecula compared to the isotropic models. The apparent modulus was reduced in both homogeneous and heterogeneous models when anisotropy was added by 4%.

3.3 Sensitivity of model to imposed anisotropy ratio

When the anisotropy ratio between the in-plane and transverse moduli was increased further for the heterogeneous model, the effects observed in the *AnisoHmg* and *AnisoHtg* models were increased (Online Resource Supplemental Fig 2). However, the effect of increasing the ratio of E_j to E_i from 2 to 3 was not as pronounced as increasing the from 1 to 2. The diminished effect of further increasing the anisotropy ratio was highlighted in the extreme values of σ_{Eq} and σ_{Hyd} (Fig. 9). The maximum σ_{Eq} increased to 5.48 MPa, which is a change of only 5% for a 150% increase in the anisotropy ratio. For comparison, a 200% increase in the anisotropy ratio previously produced a 15% increase in maximum σ_{Eq} (*AnisoHtg* vs *IsoHtg*). The muted effects due to further increasing the anisotropy ratio were more pronounced for σ_{Hyd}, which resulted in changes of − 6 and 4% for maximum and minimum σ_{Hyd}, respectively, compared to the − 25 and 25% changes observed between *AnisoHtg* and *IsoHtg*. Apparent modulus (47.6 MPa) was reduced by 2% compared to *AnisoHtg* when the anisotropy ratio was further increased.

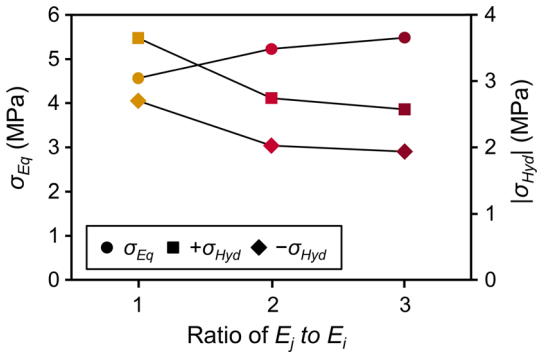

Fig. 9 Maximum von Mises equivalent stress, maximum hydrostatic stress, and minimum hydrostatic stress versus the ratio of E_j to E_i

4 Discussion

The present study reveals two separate mechanisms for shielding trabecular bone tissue from stress states leading to a propensity to damage.

Tissue elastic heterogeneity derived from tissue density was a mechanism that lead to the reduction in the von Mises equivalent stress values at negative hydrostatic stress. The shift of large values of this stress invariant from the surface elements to deep elements was realized in both the isotropic and anisotropic heterogeneous models. The surface of the trabecular bone was less dense compared to the interior of the trabeculae (Fig. 3) and therefore carried less of the applied load in both axial compression and bending. Partial volume effects inherent in μCT scans account for some of the difference in modulus, but most bone at the trabecular surface is likely truly less dense than bone deeper in the trabeculae due to the effect bone remodeling occurring only at the surface of trabeculae and continued secondary mineralization in this older tissue (Boivin et al. 2009). This result is largely in agreement with previous studies and it has been shown that heterogeneity in FE models improved their correlation with experimental data (Kaynia et al. 2015; Renders et al. 2008; Torres et al. 2016). While a previous study did not see large differences in the elastic response of trabecular bone (Gross et al. 2012), changing the magnitude and spatial distribution of stress in the model as observed here (Fig. 6 vs Fig. 7 and Online Resource Supplemental Fig 1 vs Fig. 8) will change the pressure gradients in the lacunar–canalicular network, and through mechanocoupling would likely change the fluid shear stress experienced by osteocytes altering mechanotransduction (Turner and Pavalko 1998). Therefore, in models attempting to relate stress to either bone

failure or mechanotransduction, including heterogeneity is important for accurate results due to its effect on the both the values and spatial distribution of stress.

Tissue elastic anisotropy was a mechanism that leads to a reduction in the range of hydrostatic stress and to the predictions of marginally increased maximum values of the von Mises equivalent stress compared to the isotropic trabecular bone tissue models. Increasing the ratio of anisotropy made this effect more pronounced (Online Resource Supplemental Fig 2). The combination of lower von Mises equivalent stress and reduced positive hydrostatic stress would decrease the likelihood of failure and damage due to the associated reduction in stress triaxiality. Furthermore, anisotropy in the models resulted in a system that was more stretch dominated, which would be more efficient in respect to the amount of bone tissue needed (Deshpande et al. 2001). These changes indicate that the highly anisotropic nature of trabecular bone is a strengthening mechanism acting in combination with the tissue heterogeneity and results in a more efficient structure. However, the benefit of increasing the anisotropy ratio is attenuated once into the range of ratios expected between the direction transverse to the collagen fibril plane to the two directions within that plane (Fig. 9). Thus, the accurate determination of the anisotropy ratio in trabecular bone imposed by the alignment of collagen fibrils may not be wholly necessary other than to within the general expected range, which captures the majority of the effect of local anisotropy. A somewhat benign dependence on the chosen anisotropy ratio is ideal because the accurate determination of this ratio experimentally in individual trabeculae is challenging. While there were no clear indications that there was an interactive effect between anisotropy and heterogeneity, these properties were assigned independently of one another and an additive effect is to be expected. Refining the tissue definition in the model further by varying anisotropy as a function of the distance from the trabecular surface (Georgiadis et al. 2016) would likely produce a strong interactive effect between anisotropy and heterogeneity particularly in thicker trabeculae, which likely contain more old tissue because heterogeneity is influenced by this distance as well (Fig. 2).

Nonlinear deformation, microdamage, and mechanotransduction in bone tissue have been related to von Mises equivalent stress, hydrostatic stress, and, consequently, stress triaxiality. The Drucker–Prager and Mohr–Coulomb failure criteria for the onset of nonlinear deformation in bone combine the von Mises equivalent and hydrostatic stress by a linear combination to define a pressure dependent yield criterion (Wang et al. 2008). Stress triaxiality is a fundamental parameter in continuum damage mechanics when computing the damage equivalent stress, the damage release rate, and damage evolution (Lemaitre 2012). Such concepts have successfully been applied to bone as well (Hambli et al. 2016; Mengoni and Ponthot 2010). Additionally, the distribution of von Mises equivalent stress may help drive bone remodeling (Yeni et al. 2008). Hydrostatic stress could also influence mechanotransduction by driving the movement of fluid through the lacunar–canalicular network and altering pressure gradients (Scheiner et al. 2016). Both hydrostatic and deviatoric stress components are important for fracture healing as well (Carter et al. 1998). Therefore, the accurate prediction of the von Mises equivalent stress, hydrostatic stress, and stress triaxiality is important, and the changes in the maximum values and distributions of these stress quantities reported here may explain some of the variability in predicting stress and ultimate load from μCT-based FE models when simplistic tissue properties are defined in trabecular bone (Zysset et al. 2013).

This study investigated the effect of anisotropy in trabecular bone tissue on the stress distribution in trabecular bone under uniaxial compressive mechanical loading. While the lamella of the mineralized collagen fibrils are largely aligned along the surface of trabecular bone, the direction of collagen fibrils in the plane of each lamella and between adjacent lamella varies (Georgiadis et al. 2016). While the main alignment orientation was approximated using the method presented here, the effect of the orientation of lamellae within the trabeculae was accounted for only in an average sense through the transversely isotropic elastic behavior. Bone is an orthotropic tissue, and the mechanical response along the axial direction of the collagen fibrils is different than the circumferential direction (Reisinger et al. 2011). However, the ratio between these two in-plane directions was smaller than the average ratio between these in-plane directions and the direction normal to the collagen plane (Reisinger et al. 2011). Although the indentations to determine the modulus ratios in that study was performed on cortical bone, both the microstructures of cortical and trabecular bone are composed of lamella of aligned mineralized collagen fibrils. Therefore, the ratios between modulus within and normal to the lamellar plane are expected to be similar. By assuming an in-plane (jk-plane)-to-transverse (along i-axis) modulus ratio that is between the axial and circumferential-to-radial ratios of modulus, the effect of the varying distribution of the collagen alignment within each lamella was effectively averaged out. Additionally, the effect of varying the anisotropy ratio (i.e., the ratio between the transverse local i-axis and the in-plane tissue properties) within the expected range was much smaller than the effect of assigning anisotropy in general (Fig. 9). Therefore, transverse isotropy is a reasonable approximation of the anisotropic response of trabecular bone at the microscale.

As shown in Fig. 2, small finite elements were preferentially distributed along the trabecular surface, while interior elements were larger to help reduce model size under the constraint of needing to capture the surface of the trabeculae accurately. Because the mesh density was high and there is

an benign element size dependency with second-order elements for the case of elastic deformation, the overall effect of having larger interior elements for accurately predicting stress was deemed negligible. The method utilized to define collagen fibril orientation assumed perfect alignment with the trabecular surface through the thickness of the trabeculae (Fig. 1). Due to a coarser interior mesh, the orientation alignment between adjacent elements was more varied and did not follow the trabecular surface direction with as high of a resolution, especially in regions of high surface curvature. However, this variation was not a concern because collagen fibrils are less aligned further into a trabecula (Georgiadis et al. 2016; Reznikov et al. 2015).

The principal limitation of this work is that only one μCT scan was studied, and the results may vary in samples with a different microarchitecture than those presented in Table 1, such as varying bone volume fraction, trabecular thickness, or connectivity with disease or in animal models. It is important to distinguish the fabric tensor of trabecular bone derived from its microarchitecture from the tissue anisotropy induced here within a trabecula. While varying the degree of anisotropy of the trabecular microarchitecture will likely have an effect, this would be due to the alignment or misalignment of trabeculae in the loaded direction and not due to the local distribution of stress in the trabecular tissue itself. However, due to the novel method presented here of automatically defining trabecular orientations from μCT data, the major limitation of studying the influence of sample specific anisotropy in trabecular bone can be easily overcome to allow for the detailed study of the effects of anisotropy in a wide range of conditions and parameters.

5 Conclusion

This study demonstrated the effects of tissue heterogeneity and tissue anisotropy of trabecular bone on the stress evolution under simulated mechanical loading of trabecular bone. By using a novel computational approach to calculate local orientations of individual trabeculae and automatically apply that orientation to elements within a FE model, the effects of tissue anisotropy on stresses in trabecular bone were evaluated in a sample specific continuum model. Endowing FE models with microstructurally appropriate properties (i.e., considering bone as a heterogeneous and anisotropic tissue) altered the spatial distribution of stress and the magnitude and location of their extreme values compared to the predictions from models with the common simplified assumptions of homogeneous and isotropic elastic tissue properties. Future work is needed to evaluate the effects of anisotropy over a wide range of values and microarchitectures, but due to the computational method presented here, the inability to define anisotropy is no longer a limitation of the field.

Acknowledgements This material was based upon work supported by the National Science Foundation under Grant No. 1643164.

Compliance with ethical standard

Conflicts of Interest The authors declare that they have no conflicts of interest.

References

Ashman R, Cowin S, Van Buskirk W, Rice J (1984) A continuous wave technique for the measurement of the elastic properties of cortical bone. J Biomech 17(5):349–361. https://doi.org/10.1016/0021-9290(84)90029-0

Benzley SE, Perry E, Merkley K, Clark B, Sjaardama G (1995) A comparison of all hexagonal and all tetrahedral finite element meshes for elastic and elasto-plastic analysis. In: Proceedings of 4th international meshing roundtable, Sandia National Laboratories, Albuquerque, vol 17, pp 179–191

Boivin G, Farlay D, Bala Y, Doublier A, Meunier PJ, Delmas PD (2009) Influence of remodeling on the mineralization of bone tissue. Osteoporos Int 20(6):1023–1026. https://doi.org/10.1007/s00198-009-0861-x

Burr DB (2016) The use of finite element analysis to estimate the changing strength of bone following treatment for osteoporosis. Osteoporos Int 27(9):2651–2654. https://doi.org/10.1007/s00198-016-3707-3

Carter DR, Beaupré GS, Giori NJ, Helms JA (1998) Mechanobiology of skeletal regeneration. Clin Orthop Relat Res 355(Suppl):S41–55. https://doi.org/10.1097/00003086-199810001-00006

Deshpande V, Ashby M, Fleck N (2001) Foam topology: bending versus stretching dominated architectures. Acta Mater 49(6):1035–1040. https://doi.org/10.1016/S1359-6454(00)00379-7

Engelke K, van Rietbergen B, Zysset P (2016) FEA to measure bone strength: a review. Clin Rev Bone Miner Metab 14(1):26–37. https://doi.org/10.1007/s12018-015-9201-1

Georgiadis M, Guizar-Sicairos M, Gschwend O, Hangartner P, Bunk O, Müller R, Schneider P (2016) Ultrastructure organization of human trabeculae assessed by 3D sSAXS and relation to bone microarchitecture. PLoS One 11(8):e0159,838. https://doi.org/10.1371/journal.pone.0159838

Gross T, Pahr DH, Fc Peyrin, Zysset PK (2012) Mineral heterogeneity has a minor influence on the apparent elastic properties of human cancellous bone: a SRμCT-based finite element study. Comput Methods Biomech Biomed Eng 15(11):1137–1144. https://doi.org/10.1080/10255842.2011.581236

Hambli R, Frikha S, Toumi H, Tavares JMR (2016) Finite element prediction of fatigue damage growth in cancellous bone. Comput Methods Biomech Biomed Eng 19(5):563–570. https://doi.org/10.1080/10255842.2015.1048687

Jaasma MJ, Bayraktar HH, Niebur GL, Keaveny TM (2002) Biomechanical effects of intraspecimen variations in tissue modulus for trabecular bone. J Biomech 35(2):237–246. https://doi.org/10.1016/S0021-9290(01)00193-2

Kaynia N, Soohoo E, Keaveny TM, Kazakia GJ (2015) Effect of intraspecimen spatial variation in tissue mineral density on the apparent stiffness of trabecular bone. J Biomech Eng 137(1):0110,101–0110,106. https://doi.org/10.1115/1.4029178

Kelleher JE, Siegmund T, Du M, Naseri E, Chan RW (2013) Empirical measurements of biomechanical anisotropy of the human vocal fold lamina propria. Biomech Model Mechanobiol 12(3):555–567. https://doi.org/10.1007/s10237-012-0425-4

Lemaitre J (2012) A course on damage mechanics. Springer, Berlin Heidelberg

Lips P, Courpron P, Meunier P (1978) Mean wall thickness of trabecular bone packets in the human iliac crest: changes with age. Calcif Tissue Res 26(1):13–17. https://doi.org/10.1007/BF02013227

Liu XS, Ardeshirpour L, VanHouten JN, Shane E, Wysolmerski JJ (2012) Site-specific changes in bone microarchitecture, mineralization, and stiffness during lactation and after weaning in mice. J Bone Miner Res 27(4):865–875. https://doi.org/10.1002/jbmr.1503

Mengoni M, Ponthot JP (2010) Isotropic continuum damage/repair model for alveolar bone remodeling. J Comput Appl Math 234(7):2036–2045. https://doi.org/10.1016/j.cam.2009.08.061

Patel V, Issever AS, Burghardt A, Laib A, Ries M, Majumdar S (2003) MicroCT evaluation of normal and osteoarthritic bone structure in human knee specimens. J Orthop Res 21(1):6–13. https://doi.org/10.1016/S0736-0266(02)00093-1

Reisinger AG, Pahr DH, Zysset PK (2011) Principal stiffness orientation and degree of anisotropy of human osteons based on nanoindentation in three distinct planes. J Mech Behav Biomed Mater 4(8):2113–2127. https://doi.org/10.1016/j.jmbbm.2011.07.010

Renders GAP, Mulder L, Langenbach GEJ, van Ruijven LJ, van Eijden TMGJ (2008) Biomechanical effect of mineral heterogeneity in trabecular bone. J Biomech 41(13):2793–2798. https://doi.org/10.1016/j.jbiomech.2008.07.009

Reznikov N, Chase H, Brumfeld V, Shahar R, Weiner S (2015) The 3D structure of the collagen fibril network in human trabecular bone: Relation to trabecular organization. Bone 71:189–195. https://doi.org/10.1016/j.bone.2014.10.017

Rho JY, Hobatho MC, Ashman RB (1995) Relations of mechanical properties to density and CT numbers in human bone. Med Eng Phys 17(5):347–355. https://doi.org/10.1016/1350-4533(95)97314-F

Rho JY, Kuhn-Spearing L, Zioupos P (1998) Mechanical properties and the hierarchical structure of bone. Med Eng Phys 20(2):92–102. https://doi.org/10.1016/S1350-4533(98)00007-1

Scheiner S, Pivonka P, Hellmich C (2016) Poromicromechanics reveals that physiological bone strains induce osteocyte-stimulating lacunar pressure. Biomech Model Mechanobiol 15(1):9–28. https://doi.org/10.1007/s10237-015-0704-y

Spears I, Noort RV, Crompton R, Cardew G, Howard I (1993) The effects of enamel anisotropy on the distribution of stress in a tooth. J Dent Res 72(11):1526–1531. https://doi.org/10.1177/00220345930720111101

Torres AM, Matheny JB, Keaveny TM, Taylor D, Rimnac CM, Hernandez CJ (2016) Material heterogeneity in cancellous bone promotes deformation recovery after mechanical failure. Proc Natl Acad Sci U S A 113(11):2892–2897. https://doi.org/10.1073/pnas.1520539113

Turner CH, Pavalko FM (1998) Mechanotransduction and functional response of the skeleton to physical stress: the mechanisms and mechanics of bone adaptation. J Orthop Sci 3(6):346–355. https://doi.org/10.1007/s007760050064

Van der Linden J, Birkenhäger-Frenkel D, Verhaar J, Weinans H (2001) Trabecular bone's mechanical properties are affected by its non-uniform mineral distribution. J Biomech 34(12):1573–1580. https://doi.org/10.1016/S0021-9290(01)00146-4

Vande Geest JP, Schmidt DE, Sacks MS, Vorp DA (2008) The effects of anisotropy on the stress analyses of patient-specific abdominal aortic aneurysms. Ann Biomed Eng 36(6):921–932. https://doi.org/10.1007/s10439-008-9490-3

Wang X, Allen MR, Burr DB, Lavernia EJ, Jeremiç B, Fyhrie DP (2008) Identification of material parameters based on Mohr–Coulomb failure criterion for bisphosphonate treated canine vertebral cancellous bone. Bone 43(4):775–780. https://doi.org/10.1016/j.bone.2008.05.023

Yeni YN, Zelman EA, Divine GW, Kim DG, Fyhrie DP (2008) Trabecular shear stress amplification and variability in human vertebral cancellous bone: relationship with age, gender, spine level and trabecular architecture. Bone 42(3):591–596. https://doi.org/10.1016/j.bone.2007.11.011

Zysset PK, Dall'Ara E, Varga P, Pahr DH (2013) Finite element analysis for prediction of bone strength. Bonekey Rep 2:386. https://doi.org/10.1038/bonekey.2013.120